Biomechan Model Mechanobiol (2008) 7:203–214
DOI 10.1007/s10237-007-0086-x

ORIGINAL PAPER

Part I: A novel in-vitro system for simultaneous mechanical stimulation and time-lapse microscopy in 3D

G. P. Raeber · J. Mayer · J. A. Hubbell

Received: 9 December 2006 / Accepted: 4 April 2007 / Published online: 9 May 2007

Abstract To investigate the migration response of cells to changes in their biophysical environment, a novel uniaxial cell stimulation device (UCSD) has been designed and tested. The device is capable of applying very precise user-defined static or dynamic mechanical stimuli in a physiologically relevant strain window (up to 50%) and frequency bandwidth (up to 2 Hz) to cells residing in a three-dimensional (3D) environment while single-cell migration is simultaneously measured by time-lapse microscopy. The system is an advancement over uniaxial loading devices reported to date in that it allows temporal and spatial quantification of migration as a function of the micromechanical environment. We make use of the favorable physical and biological properties of poly(ethylene glycol) hydrogels as model matrix and present a method for fabricating cell-containing hydrogel constructs. The 3D strain field within these constructs is modeled by finite element analysis. Fibroblasts reversibly altered their morphology and orientation in response to the strain field. In the succeeding companion paper we then exploit the system to analyze fibroblast motility induced by different stimulation regimes (refer to part II).

Keywords Mechanical stimulation · Cell migration · PEG hydrogels · Stage incubator

G. P. Raeber · J. A. Hubbell (✉)
Institute of Bioengineering and Institute of Chemical Sciences and Engineering, Ecole Polytechnique Fédérale de Lausanne (EPFL), LMRP, Station 15, 1015, Lausanne, Switzerland
e-mail: jeffrey.hubbell@epfl.ch

J. Mayer
ETeCH GmbH, Schlieren/Zurich, Switzerland

Present Address:
G. P. Raeber
Institut Straumann AG, Basel, Switzerland

1 Introduction

Mechanical cues modulate almost all cell functions, including migration. Cells sense and actively probe the biophysical state of their environment via mechanosensors and convert these signals into a biological response, a process termed mechanotransduction (Alenghat and Ingber 2002). Distinct cellular structures have been proposed as mechanosensors, including integrins (Katsumi et al. 2004), the cytoskeleton (Ingber 1997), and stretch activated enzymes or ion channels (Sachs and Morris 1998). Strikingly, both integrins and the cytoskeleton are at the same time critically involved in migration. Actinomyosin-generated forces are responsible for the internal prestress and active cell contraction (Sheetz et al. 1998), whereas coordinated binding and release of extracellular matrix (ECM) ligands via integrins transform this prestress into a net force enabling directed cell movement. As a result, integrins and the cytoskeleton fulfill a dual function in cell migration, serving as sensors and actuators simultaneously. This has important implications for the mechanobiology of cell migration: the same intracellular pathways may be involved in directing the execution of cell movement and in mechanotransduction. Furthermore, this suggests that in pathologies depending on cell migration (e.g. cancer dissemination or migration of smooth muscle cells in atherosclerosis) biophysical cues might play a determinant role. Consequently, the quantitative investigation of the migratory response of cells to mechanical cues is of substantial interest in mechanobiology.

In vivo, cells are constantly subjected to time-variant mechanical stress exerted from the ECM and neighboring cells via transmembrane receptors to the internal structures of the cell body. In some tissues, the emerging stresses follow a cyclic pattern (e.g. in the myocardium, in lung tissue or in the vessel wall), while in others they depend on the kinetic

state of the organism (e.g. in tendon, muscles, or skeletal tissues). Most tissues remodel in response to applied mechanical stress and undergo changes in form and composition until an acceptable stress state is reestablished. Tissue remodeling often involves cell migration. Hence, to investigate the transient migration response to changes in the mechanical microenvironment in vitro, an experimental model system must enable dynamic alterations in the stress state of the cell's surroundings and simultaneously allow the quantitative assessment of cell migration. To date, the method of choice for recording and analyzing single cell migration is time-lapse microscopy.

Many experimental models have been developed to mechanically stimulate cells in vitro (recently classified and reviewed by (Brown 2000)). Stretching cell-seeded elastic membranes has led to significant insights and advances in mechanobiology (Banes et al. 1990; Buckley et al. 1988; Carvalho et al. 1994; Duncan and Hruska 1994; Matsuda et al. 1998; Nishioka et al. 1993; Putnam et al. 2001). Nevertheless, the strain field imposed on cells by these setups is in most cases not representative for an in vivo situation (Basso and Heersche 2002; Duncan and Turner 1995). Therefore, systems have been engineered that create a three-dimensional (3D) strain field either by uniaxial (Akhouayri et al. 1999; Bruinink et al. 2001; Cacou et al. 2000; Eastwood et al. 1994; Langelier et al. 1999) or biaxial (Knezevic et al. 2002; Mitchell et al. 2001) stretch. Diverse biomaterials, including the natural polymers collagen and fibrin, have been used as 3D cell carriers to transduce the mechanical signals to adherent cells. However, none of these systems allowed state-of-the-art quantification of migration by 3D time-lapse microscopy of multiple pre-defined locations within several samples and the simultaneous application of user-defined displacement waveforms under controlled environmental conditions.

This work describes the design and testing of a new device, fulfilling these demands. The uniaxial cell stimulation device (UCSD) applies controlled static or dynamic mechanical stimuli to cells residing within 3D constructs and is able to acquire time-lapse sequences at the same time. Combining the features of the UCSD with the previously established technique of quantitative migration analysis from time-lapse sequences (Raeber et al. 2005), we introduce a sophisticated system that allows the correlation between migration and the biophysical environment. Additionally, we make use of the controllable biological features (Lutolf et al. 2003a,b) and the favorable mechanical material properties (Raeber et al. 2005) of poly(ethylene glycol) (PEG) hydrogels and present a technique permitting the fabrication of hydrogel constructs that offer stable supports for load transmission. These hydrogels contain PEG macromers as an inert structural platform, protease-sensitive peptides as elastically active linkers, and pendantly grafted integrin-binding peptide ligands. Hence, the incorporated peptides render these hydrogels cell-adhesive and degradable by cell-secreted enzymes, allowing cells to migrate and remodel the matrix on demand. We point out that the materials are not identical in all regards to the natural extracellular matrix, for example in that the PEG-based hydrogel is spatially homogeneous, whereas the native extracellular matrix may contain adhesion ligands in nanoscopic clusters; as such, the connections between the cell and its 3D substrate are not entirely native. We model the strain field within these constructs by finite element analysis and show that fibroblast morphology reacts in a dynamic manner to the externally imposed strain field. The succeeding companion paper (refer to part II) further exploits the system and presents detailed results on 3D fibroblast migration as a function of mechanical stimulation regimes.

2 Materials and methods

2.1 The uniaxial cell stimulation device (UCSD)

(a) A novel device that allows the simultaneous uniaxial mechanical stimulation of cells residing within 3D hydrogel constructs and continuous time-lapse microscopy was designed, manufactured and tested. The UCSD design is based on the following criteria: With regard to its *general design*, we require (a) that its dimensions allow the use of the system on conventional microscope stages; (b) for convenience a 2-part design, consisting of cell chamber and attachable mechanical stimulation unit (e.g. stand-alone use of the cell chamber for static time-lapse microscopy); (c) that it possess its own environmental system independent of an incubator; (d) for practicality that it possess an axisymmetrically constructed cell chamber to facilitate manufacturing; and (e) that the design be suitable to hold at least two samples. With regard to *mechanical stimulation*, we require (a) static and dynamic application of uniform, homogeneous uniaxial stretch to cells cultured within soft hydrogels, textiles or comparable structures; (b) precise control of the strain magnitude, max strain of 50% ($\varepsilon_{\max} \geq 1.5$); (c) precise control of any desired waveform of a periodical or cyclic stimulation; (d) high repositioning accuracy to allow repetitive imaging of the same volume; (e) stimulation frequency of 2 Hz or more; and (f) application forces of 25 N or more. From the perspective of *imaging and microscopy*, we require (a) fully automated repetitive image acquisition from multiple locations within the constructs enabling time-lapse microscopy; (b) simultaneous mechanical stimulation and time-lapse microscopy requiring integration of image acquisition and motion control (three microscope axis and one mechanical stimulation actuator); (c) designed for transmitted *or* reflected light microscopy; and (d) optical properties that allow the use of fluorescence. Finally, from the perspective of *cell culture*,

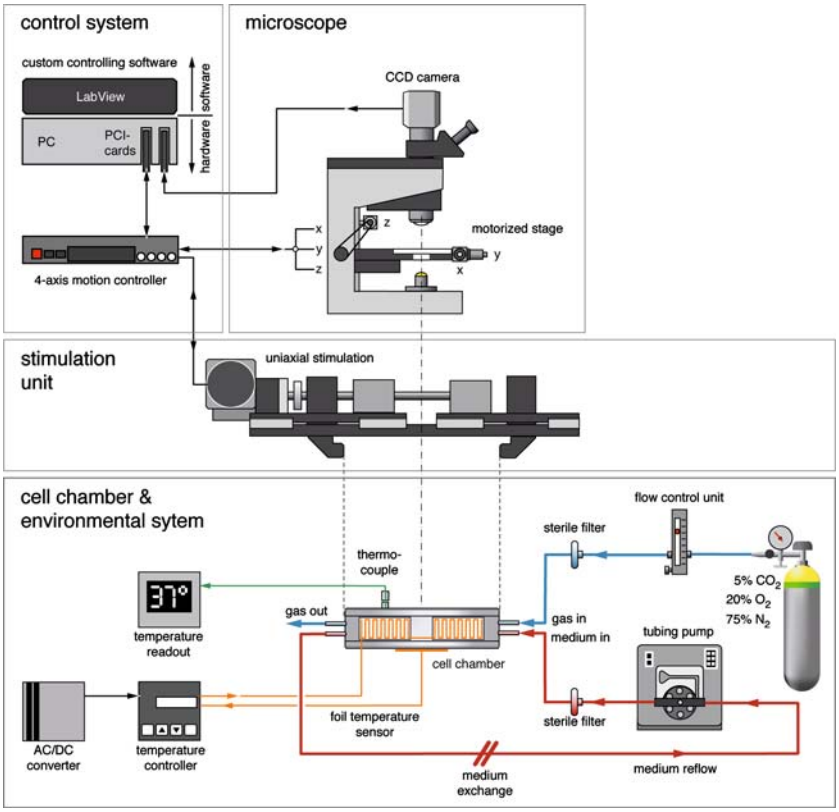

Fig. 1 Components of the UCSD system. The cell chamber is connected to the environmental system for controlled maintenance of cell culture conditions. The mechanical stimulation unit is mounted on top of the cell chamber and transmits an accurate uniaxial movement to the cell-populated samples inside the chamber. For simultaneous mechanical stimulation and microscopical observation, the cell chamber and the stimulation unit are fixed to the motorized stage of an inverted microscope. Time-lapse sequences of multiple locations within the samples are recorded by a CCD camera. Motion and vision of the UCSD system are integrated by the control system driving the stepper motors and triggering image acquisition

we require that the device be (a) qualified for long-term experiments (prove non-cytotoxicity of all components, show temperature and pH stability, enable long-term sterility); (b) the possibility of cell maintenance without compromising predefined observation locations; and (c) that all components in contact with cell culture be autoclavable

2.2 Principal components of the UCSD system

Based on the above listed design criteria the setup depicted in Fig. 1 was developed. It consists of the following five main components: (1) the cell chamber and its parts, constituting the core of the system that holds the samples; (2) the mechanical stimulation unit that can be mounted on top of the cell chamber; (3) the microscope with the motorized stage and the flanged CCD camera; (4) the environmental system responsible for maintaining temperature within the chamber and permitting medium and gas exchange; and (5) the control system with custom software, integrating motion control and image acquisition.

2.2.1 Cell chamber

The cell chamber features the characteristics of a small incubator with optical accessibility of the samples by any conventional inverted or upright microscope. An exploded drawing of the cell chamber and its components is shown in Fig. 2. The setup uses an inverted microscope to acquire brightfield images. The samples are accordingly located close to the bottom observation window and are illuminated through the upper window. The cross-section of the chamber is designed such that the medium filling the chamber is in direct contact with the upper window, thereby reducing the number of interfaces the illuminating light has to pass. At the same time, an air-filled volume is formed, allowing the use of CO_2 buffered media. The shell of the chamber has a diameter of 130 mm and is composed of three main parts made of titanium grade two: the bottom plate with the embedded bottom observation window, the top plate, holding the upper window, and the middle ring with a recess on each side for the transmission of the symmetrical deflection. The bottom and top plate have an in-ground silicone seal ring (Hitec MVQ 55; FDA approved for used with pharmaceuticals and food processing, Angst & Pfister, Zurich, Switzerland) and are screwed to the middle part with six countersinks. A 200 µm thick highly flexible silicone membrane (medical grade silicone; Medic Service AG, Tagelswangen, Switzerland), fixed by a frame to the middle ring, constitutes the interface between the cell chamber and the moving part of the mechanical stimulation unit. The deflection is transmitted via a permanent magnet through the membrane to the magnet counter block, flanged to the polyetheretherketone

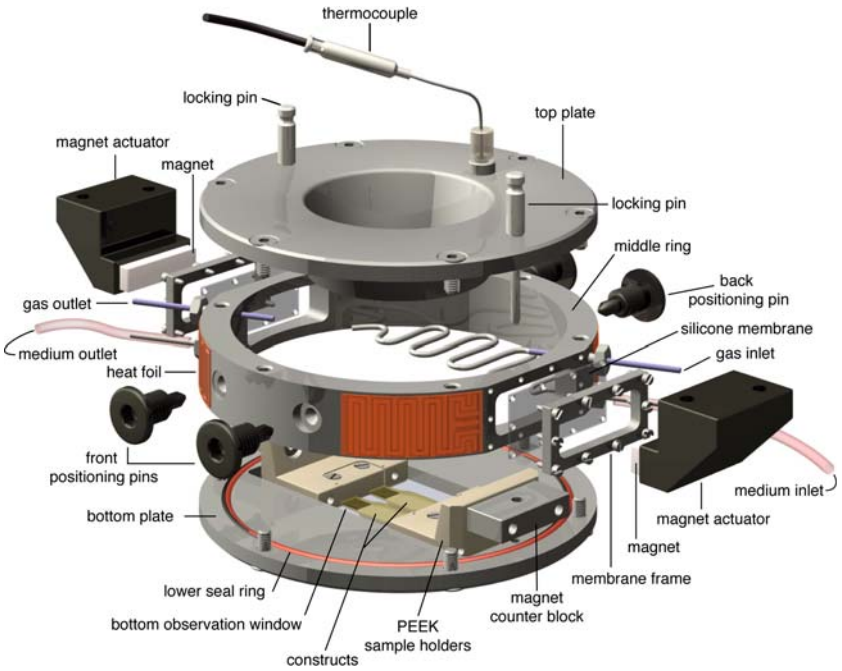

Fig. 2 Exploded view of the cell chamber equipped with two hydrogel constructs showing all relevant components (black parts belong to the stimulation unit). The three main parts of the shell are made of titanium: the top plate, the middle ring, and the bottom plate. The samples are observed and illuminated through the bottom and the top window. The uniaxial mechanical stimulation is transmitted from the magnet actuator by a NdFeB magnet through the silicone membrane to the magnet counter block and finally via the PEEK sample holders to the cell populated hydrogel constructs. The assembled chamber is fixed to the stimulation unit by front and back positioning pins centering in countersinks of the middle ring. The locking pins obviate the dislocation of the sample holders during the coupling procedure of the magnets and are replaced with plugs for normal operation. The chamber is provided with inlets and outlets for medium and gas exchange and kept at constant temperature by six heat foils

(PEEK, TecaPEEK; Ensinger, Nufringen, Germany) sample holders inside the chamber. With this design, it was possible to hermetically seal the cell chamber despite the moving parts and thereby increase the sterility to a level where long-term experiments are practicable.

The clamping force is applied by two sintered Neodymium–Iron–Boron (NdFeB) magnets with the dimensions 30 × 10 × 6 mm (N35; Maurer Magnetic, Grüningen, Switzerland). NdFeB magnets have a very high energy density but contain free neodymium as part of their structure and are, therefore, highly prone to corrosion. As a consequence, the magnets are only used outside of the chamber and painted with a protective coating. Inside the cell chamber, a magnetizable X5CrNiCuNb16-4 steel with very good corrosion resistance (N 700 ESU; Böhler & Co. AG, Wallisellen, Switzerland) is utilized as the magnets' counterparts. The clamping force through the silicone membrane of an individual magnet-counterblock pair was determined on a commercial tensile tester (Zwicki; Zwick GmbH, Ulm, Germany) with a 50 N load cell. The two borosilicate windows with broadband anti reflection coating (Filtrop AG, Balzers, Liechtenstein) are bonded to the titanium frame with a silicone adhesive (Elastosil E41; Angst&Pfister, Zurich, Switzerland), have a thickness of 1.1 mm, allow microscopic observation, illumination, and serve as slide for the PEEK sample holders. The tribological pairing of glass and PEEK in an aqueous environment features a low sliding friction rendering other bearings unnecessary. The optical properties of the observation windows allow fluorescence microscopy above 330 nm. The chamber has two inlets and two outlets for gas and medium exchange, a tapped through hole for an internal thermocouple, and two sealed openings for locking pins. Heat foils accomplish temperature control of the chamber. All components of the cell chamber including connectors are manufactured from materials that allow steam sterilization at 125°C, 2 bar for 1 h.

2.2.2 Mechanical stimulation unit

The mechanical stimulation unit performs a symmetrical, uniaxial, high precision movement of the two magnets in opposite directions and can be attached to the cell chamber by front and back positioning pins centering in countersinks of the middle ring of the chamber. It is capable of exerting tensile or compressive loads to the samples within the cell chamber. A sectional drawing of the stimulation unit attached to the cell

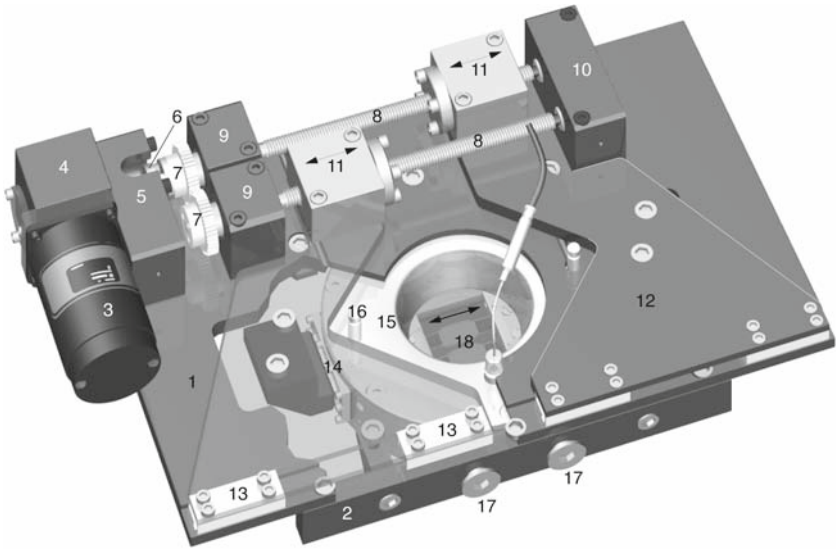

Fig. 3 Cutaway drawing of the mechanical stimulation unit fixed to the cell chamber (*15*). The components are assembled on a supporting aluminum plate (*1*) and a subjacent frame (*2*) that bears on the microscopy stage. The other components are: (*1*) supporting plate, (*2*) supporting frame, (*3*) stepper motor, (*4*) 25:1 worm gear, (*5*) motor block, (*6*) spring coupling, (*7*) counter rotating gears, (*8*) planetary roller screw, (*9*) needle bearing, (*10*) angular-contact thrust ball bearing, (*11*) nut of the planetary roller screw, (*12*) moving cantilever, (*13*) carriage guideway, (*14*) magnet actuator, (*15*) cell chamber, (*16*) locking pin, (*17*) chamber fixation, and (*18*) hydrogel constructs. Function, force flow, and individual components are described in the text

chamber is shown in Fig. 3. The individual components are assembled on an aluminum support (Fig. 3, pos. 1 and 2). The stepper motor (Fig. 3, pos. 3, ZSS 43.200; Phytron GmbH, Gröbenzell, Germany) is flanged to a worm gear (Fig. 3, pos. 4, 25:1; Hilba, Villmergen, Switzerland) and connected by a spring coupling (Fig. 3, pos. 6) to two counterrotating gears (Fig. 3, pos. 7). The spring coupling (FKZS 1225; Schlaps GmbH, Birkenau, Germany) compensates slight axis offsets and protects the system from overload. The gears are connected to high precision planetary roller screws (Fig. 3, pos. 8, INA RGT 8.5.100; Hydrel AG, Romanshorn, Switzerland) that are held by needle and angular-contact thrust ball bearings (INA NK 6/10TN and ZKLN 0624-2RS; Hydrel AG) located in supporting aluminum blocks (Fig. 3, pos. 9 and 10). This setup transforms the rotation of the stepper motor into a linear movement. A full step (1.8°) results in a movement of 0.497 µm. The stepper motors are operated in 10-times microstepping (2,000 steps/rev) mode. Each nut of the planetary roller screws (Fig. 3, pos. 11) is flanged to an aluminum cantilever (Fig. 3, pos. 12) resting on two carriage guideways (Fig. 3, pos. 13, NDN 2-40.30; Schneeberger, Roggwil, Switzerland) acting as counter bearings. The magnet actuators (Fig. 3, pos. 14) are screwed to these plates and transmit the linear movement via the sample holders to the cell-seeded constructs (Fig. 3, pos. 18) inside the cell chamber (Fig. 3, pos. 15). The only contact area between the cell chamber and the mechanical stimulation unit are the tips of the positioning pins. Consequently, the heat loss from the chamber via the stimulation unit is minimized.

2.2.3 Microscope

The cell chamber is mounted with or without mechanical stimulation unit on an inverted microscope (Labovert FS; Leitz, Wetzlar, Germany). The microscope is equipped with a custom-made motorized xy-stage and a z-axis drive (stepper motors were from Phytron GmbH, Gröbenzell, Germany). For image acquisition, a CCD camera attached to the c-mount (Basler A101, 1, 300 × 1, 030 pixel, 12 fps, 2/3 in. progressive scan CCD; Basler AG, Ahrensburg, Germany) is used in conjunction with a 10× objective. The optical resolution of the system equipped with a 10× objective was between 1 and 2 µm as determined with a Richardson test slide (SPI, West Chester, PA, USA).

2.2.4 Environmental system

The environmental system is responsible for maintaining cell culture conditions in the chamber. It is schematically depicted in Fig. 1 and is composed of the heating system, the tubing pump for medium exchange, and the gas flow-through system. The chamber is heated by six heat foils (Minco, Minneapolis, MN, USA) bonded with a silicone adhesive (RTV-6; Minco) to the outer surface of the chamber. Two foils are located at the bottom plate and four at the outer perimeter of

the middle ring. For closed loop temperature control, a foil resistor thermocouple (Pt100; Minco) is bonded to one of the heat foils at the bottom plate. The signal of the thermocouple is fed to a PID controller (CT15; Minco) that regulates the solid state relay between a AC-DC converter (LWN 1601-6R, 250 W; Power-One, Uster, Switzerland) and the heating foils. Additionally, the temperature of the medium is measured above the lower observation window, close to the constructs with a ϕ 1 mm thermocouple (Type J; Thermocontrol GmbH, Dietikon, Switzerland).

A considerable heat loss through the relatively large observation windows was anticipated. To reduce local temperature differences in the medium, forced convection is induced by circulating the medium in closed circuit. A tubing pump (MC-MS/CA4; Ismatec SA, Glattbrugg, Switzerland) aspirates medium above the lower observation window (heat sink) and recirculates it with a flow rate of 3 ml/min through a meandering stainless steel tubing located inside the chamber above a heat foil (heat source). Thereby, a slow but steady flow of warmer medium into colder regions is ensured. To exchange the medium, the loop is opened and old medium is replaced with pre-warmed fresh medium.

The 5% CO_2 environment is maintained with a constant flow of a gas mixture (5% CO_2, 20% O_2, 75% N_2, Carblood; Carbagas, Zurich, Switzerland) through the chamber. A flow meter (1100 V-A-A-150; Wisag, Zurich, Switzerland) regulates the flux to 20 ml/h. Gas and medium inlets are equipped with a 0.22 μm pore diameter sterile filters.

2.2.5 Control system

The four stepper motors of the UCSD system are actuated by a 4-axis stepper motor drive (MID-7604; National Instruments, Austin, TX, USA) accessed through a 4-axis motion controller board (PCI-7344; National Instruments) inside a Pentium III PC running Windows NT (see Fig. 1). Frames from the CCD camera are grabbed by an image acquisition board (PCI-1422; National Instruments) and written to hard disks for off-line image analysis. For the control of the UCSD system several interconnected custom software modules were implemented in LabView v6 extended with the vision development kit (National Instruments, Austin, TX, USA). With this platform it is possible to integrate 4-axis motion control and image acquisition.

2.3 PEG derivatives and peptides

Branched 4arm-PEG macromers, 20 kDa, were purchased from Shearwater Polymers (Huntsville, AL, USA) and functionalized at the OH-terminus. Divinlyl sulfone was from Aldrich (Buchs, Switzerland). PEG vinyl sulfones (PEG-VS) were synthesized and characterized as previously described (Lutolf and Hubbell 2003). Peptides were synthesized on solid resin using an automated peptide synthesizer (PerSeptive Biosystems, Farmington, MA, USA) with F-moc chemistry. Purification was performed by C18 chromatography (Biocad 700E; PerSeptive Biosystems) and peptides were analyzed by mass spectrometry (MALDI-TOF). All standard peptide synthesis chemicals were analytical grade or better and were purchased from Novabiochem (Läufelfingen, Switzerland).

2.4 Cell culture

Human foreskin fibroblasts (HFFs; neo-natal normal human dermal fibroblast; Clonetics, San Diego, CA, USA) were cultured in fibroblast cell culture medium (Dulbecco's Modified Eagle's Medium, with 10% fetal bovine serum (FBS) and 1% antibiotic-antimycotic, all Gibco BRL, Life Technologies, Grand Island, NY, USA) at 37°C and 5% CO_2. Cells were removed from culture substrates using 0.05% trypsin/0.02% EDTA (Gibco BRL), centrifuged at 400 g for 5 min, and resuspended in culture medium.

2.5 Cytotoxicity testing of the cell chamber

The cytotoxicity of the cell chamber was tested by comparing cell viability of HFFs cultured within the chamber with daughter cells cultured in 24-well plates in an incubator under standard conditions. Cell viability was measured by a colorimetric assay based on the cleavage of the tetrazolium salt WST-1 by mitochondrial dehydrogenases according to the manufacturers instructions (WST-1, Roche Diagnostics GmbH, Mannheim, Germany). HFFs from subconfluent cultures at passage P9 were seeded onto etched (1 M NaOH for 1 h), cleaned, and sterilized circular borosilicate glass cover slips (ϕ 12 mm, 0.17 mm thickness) at a density of 5,000 cells/cover slip. After 24 h, the cell carriers were transferred either into the cell chamber or into individual wells of a 24-well plate and cultured for up to 96 h. Medium was exchanged after 2 days in both cultures. After 12, 24, 48, 72, and 96 h, carriers from control and cell chamber cultures were transferred into a new 24-well plate and the mitochondrial activity was measured by WST-1. The experiment was conducted twice and four samples were assayed for each time point and condition. Student's-*t* tests were made to determine the *p*-values between the two conditions. The pH was concurrently measured for both conditions.

2.6 Casting of PEG hydrogel constructs

PEG hydrogels were used as model matrix to study cell migration in a biophysically and chemically controlled 3D environment. PEG hydrogel precursor solutions contained ~32 μM integrin-binding peptides Ac-GCGYG*RGDSP*G (adhesion domain shown in italic) (Hern and Hubbell 1998;

Pierschbacher and Ruoslahti 1984) and were rendered degradable by matrix metalloproteinases (MMPs) by crosslinking the PEG macromers with a bifunctional MMP-sensitive peptide sequence (e.g. Ac-GCRD-GPQG↓IWGQ-DRCG, where ↓ indicates the cleavage site) (Lutolf et al. 2003a). The PEG materials used herein had a precursor concentration of 10% and a stoichiometric ratio of 0.83 (molar ratio of VS and SH groups, see (Lutolf and Hubbell 2003)). HFFs were added to the PEG precursor solution and had a concentration of 10^5 cells/ml after gelation and swelling. To enable the clamping of the very fragile cell-populated hydrogels to the carriages of the cell chamber, stainless steel meshes were cast into the hydrogel in a process similar to injection molding.

The mold consisted of two main stainless steel parts, held together with six screws, a polytetrafluoroethylene (PTFE) membrane, and a PTFE inlay (see Fig. 4). The crosslinking reaction was carried out in the mold holding two CrNi stainless steel meshes in place, which were cast-in upon polymerization. The meshes had a filament thickness of 210 µm, a mesh opening of 550 µm, and were held in place in the mold by silicone spacers. Prior to use, the meshes were washed in ethanol and micropure water. Additionally, to increase adhesiveness, they were oxygen-plasma activated and simultaneously sterilized for 15 min (Plasma Cleaner/Sterilizer PDC-32G, Harrick, Ossining, NY, USA) shortly before the casting procedure. The mold was vapor sterilized, assembled under sterile conditions and warmed up to 37°C before the precursors were mixed and injected into the mold. After 12 min of curing at 37°C, the upper part of the mold including the PTFE membrane was removed and the construct supported by the PTFE inlay were collectively separated from the bottom plate. The inlay served as a carrier for the transfer of the fragile construct into a petri dish containing prewarmed cell culture medium. With this procedure it was assured that the constructs were not subjected to external strains prior to the actual experiments. The constructs were cultured under free floating conditions for approximately 48 h before they were installed in the cell chamber for succeeding experiments.

2.7 Finite element (FE) analysis

Strain and stress analysis of the PEG constructs was performed using the Patran/Marc software suite of programs (MSC Software Corporation, Redwood City, CA, USA). A deformation was imposed that was representative of the deflection applied by the UCSD, i.e. up to 10% elongation. The model consisted of 3D quad elements connected through a P-Shell formulation, restraints were applied by the removal of the u_x, u_y, u_z, f_x, f_y, and f_z degrees of freedom along the grounded side of the model. The material was modeled as an isotropic, ideal elastic, incompressible Hookean solid ($\nu = 0.5$). The deformation was applied as uniform translation acting out from the model edge. Material properties corresponding to those measured rheometrically were utilized, i.e. $G' = 150$ Pa, G'' = negligible.

3 Results and discussion

3.1 Cell chamber design and performance

The cell chamber depicted in Fig. 2 is designed to fit onto different microscopes (Leitz Labovert, Zeiss, Axiovert 135, Leica DM-IRBE and others) and can be used in various laboratory setups as a stage incubator. With the environmental system connected (Fig. 1), the cell chamber can be operated independent of an incubator and offers controlled cell culture conditions with excellent optical accessibility for transmission or reflection microscopy. Its size and form is a trade-off between the limited space available on a microscopy stage, the number of samples that can be investigated simultaneously, and the manufacturing technique (axisymmetry). The chamber provides room for two to maximally three constructs. Many comparable systems work only with one sample (Eastwood et al. 1998; Kim and Mooney 2000; Langelier et al. 1999; Mitchell et al. 2001). However, all samples share the same medium, which can compromise results obtained from an individual construct due to interaction via soluble signaling molecules secreted from a neighboring construct. The relatively large medium volume of 30–50 ml needed to fill the chamber and the constant agitation is advantageous in this respect since it reduces and levels the concentration. On the other hand, if one wants to investigate soluble factors that are sequestered by the cells as a function of the mechanical stimulation (e.g. proteases (Prajapati et al. 2000) or growth factors (Tang et al. 2004)), the proteins need to be extracted and concentrated from a large volume (e.g. by dialysis). We have assayed the gelatinolytic activity of concentrated supernatants by gelatin zymography and have found this procedure to work well despite the initial dilution. For certain time-dependent studies, it might be advantageous that the system facilitates continuous media sampling.

The design of a load-transmitting interface between the sterile chamber inside and the outside by a magnetic clutch enabled us to engineer a hermetically sealed reactor with very stable environmental conditions and excellent long-term sterility. The sample holders allow for a wide range of substrates such as membranes, textiles or 3D hydrogels constructs with a suitable mounting to be fixated. The central cone of the top plate provides room for the illumination cone of inverted microscopes and at the same time is partially immersed in the medium, increasing the illumination efficiency and the quality of transmission images. Concurrently, an air–liquid interface is formed inside the chamber allowing

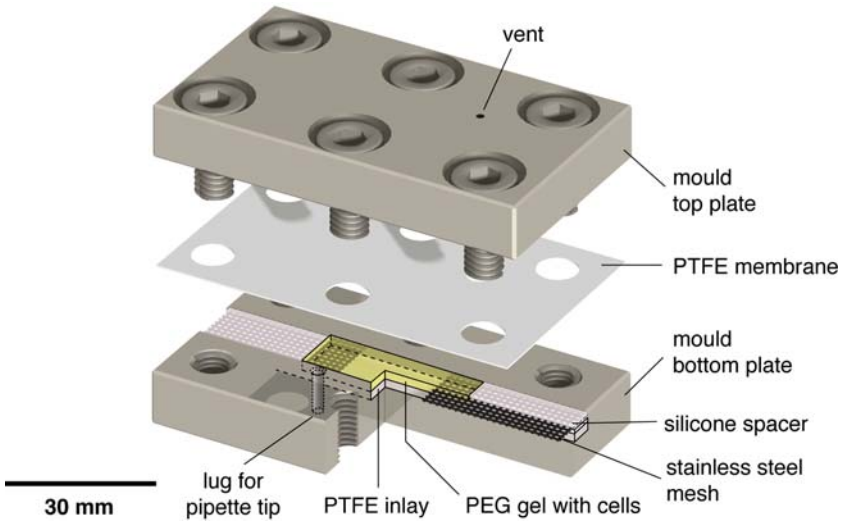

Fig. 4 Exploded view of the mold designed for casting PEG hydrogel constructs. The two stainless-steel meshes are held in place by silicone spacers. After assembly of the mold, the precursor solution containing the cells is injected into the lug at the bottom plate. Displaced air can escape via the vent. After curing, the PTFE membrane and the PTFE inlay facilitate the removal of the construct from the mold

the use of a cell culture medium with a CO_2-dependent buffer. Temperature stability over time and spatial distribution was achieved by a foil heating system in combination with forced convection by recirculating the medium with a flow rate of 3 ml/min. With this setup, local temperature differences were below 0.1°C and the mean medium temperature measured in the inlet region was 37.2 ± 0.2°C during a 48-h test. However, circulating medium could exert shear stresses on cells, known to influence cell behavior (Barakat and Lieu 2003). An estimate of the unidirectional fluid shear stress τ was calculated for the unlikely "worst case" that the entire flow is confined to a volume above a single construct by the equation $\tau = 6\mu Q/bh^2$ where Q is the flow rate, μ is the dynamic viscosity of the medium (approximated by the value for water), and b and h are the width of the construct and height of the flow channel above the construct, respectively. A flow rate of 3 ml/min causes a fluid shear stress on the surface of a single construct of less than $1‰$ of a normally used shear stress of 2 N/m^2 to induce cellular reactions (Lee et al. 2002). Additionally, the cells in our setup are encapsulated within the 3D gel substrate. Therefore, fluid shear stresses caused by the forced convection are considered negligible.

To ensure optimal cell performance, the non-cytotoxicity of the various materials in contact with medium was tested. To this end, the mitochondrial activity of HFFs cultured within the cell chamber was measured over a 96-h period and compared to incubator controls (see Fig. 5). No statistically significant differences were detected. Therefore, the cell chamber offers equal cell culture performance as a commercial incubator. Furthermore, no bacterial or fungal contamination was observed in a 2-week experiment without antibiotic or antimycotic additives in the medium. In conclusion, the cell chamber fulfills the predefined design criteria and presents a sophisticated small incubator unit for sterile long-term microscopic observation like time-lapse microscopy.

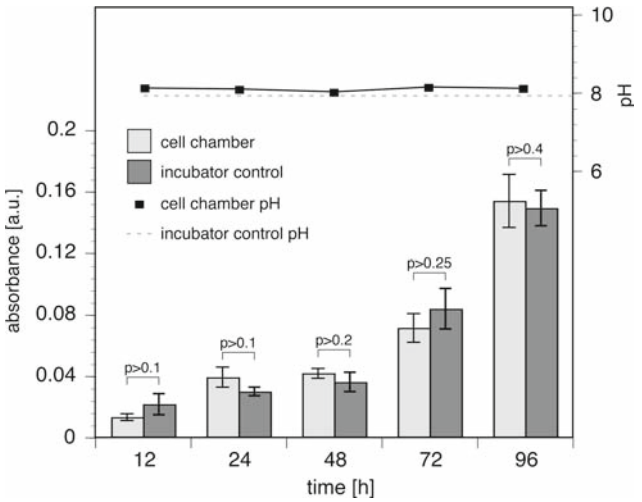

Fig. 5 The metabolic activity of HFFs grown in the cell chamber was measured as an indication for optimal environmental conditions and cytotoxicity (lower part of the graph). The data was compared to cultures grown in the incubator (incubator control). Statistical analysis showed no significant difference over the measurement duration of 4 days. The upper part of the graph shows the pH of the cell chamber medium

3.2 Mechanical stimulation unit design and performance

The mechanical stimulation unit is built as a separate device and can be attached on top of the cell chamber (Fig. 3). This 2-part setup increases the flexibility of the system. We chose to build a stimulation unit that applies a symmetrical, uniaxial stretch to the samples clamped to the samples holders inside the cell chamber. The stimulation unit applies highly

precise deformations. The repositioning error of the sample holders with mounted hydrogel constructs is below the resolution limit of the 63× objective used to determine the position of the sample holders edge (< 0.5 µm). As a caveat, it should be noted that this system is an open-loop, displacement-driven system, with no force monitoring. In rheological measurements, the storage modulus G' of the PEG hydrogel was 180 Pa (data not shown), corresponding to a Young's modulus of ∼550 Pa (assuming $\nu = 0.5$). Accordingly, only minimal forces were required to be transmitted by the magnetic clutch. However, in the case where stiffer materials need to be deformed, the elastic deformation of the 200 µm thick silicone membrane has to be taken into account. The maximal tractive force transmitted by the magnetic clutch was measured on a tensile tester and fulfilled, with 35 N, the design criterion. Compression loads can be much higher and are only limited by the torque of the stepper motor (200 mNm, 25× increased by the worm gear).

Stepper motor usage allows great versatility of input waveforms. The sole limiting factor of the presented load transmission system is the restricted frequency bandwidth. Due to the relatively complex design, the inertia of moving parts is considerable. The maximum stimulation frequency of the UCSD is ∼2.0 Hz and was measured on the whole system for a sinusoidal movement with an amplitude of 5 mm (on one side, corresponding to 50% stretch). This frequency is similar to that of other stimulation devices (Jones et al. 1991; Kim and Mooney 2000) and is sufficient for most applications including the simulation of the pulsatile blood flow (Fung 1990, 1993; Ku and Zhu 1993; Patel et al. 1965). From the neutral position, both carriers can move 5 mm inward or 5 mm outward. Thus, a 20 mm construct (see Fig. 6 for construct) that is mounted (unstretched) while the carriers are positioned close together (2 × −5 mm) will then be stretched to maximally 40 mm (20 mm + 4 × 5 mm), corresponding to 100% elongation. In conclusion, the mechanical stimulation unit can provide very precise symmetric uniaxial ramp or cyclic stimulation with various waveforms, frequencies up to 2 Hz and a maximal elongation of 20 mm.

3.3 Fabrication and performance of hydrogel constructs

In this report we used HFF-populated PEG hydrogel constructs fabricated in a mold (see Figs. 4, 6) and subjected them to uniaxial deformation. This setup has several advantages over a 2D setup especially since the biomechanical microenvironment is closer to an in vivo situation where the cells are subjected to a bi- or triaxial strain field (Fung 1993; Turner et al. 1995). Uniaxial stretch produces a biaxial strain on the cells embedded within the construct due to the transversal contraction of the material. This contraction is characterized by the Poisson's number ν (incompressible materials: $\nu = 0.5$). The hydrogel is perfectly transparent, thus allowing the microscope to be focused anywhere within the depth of field of the utilized optical system.

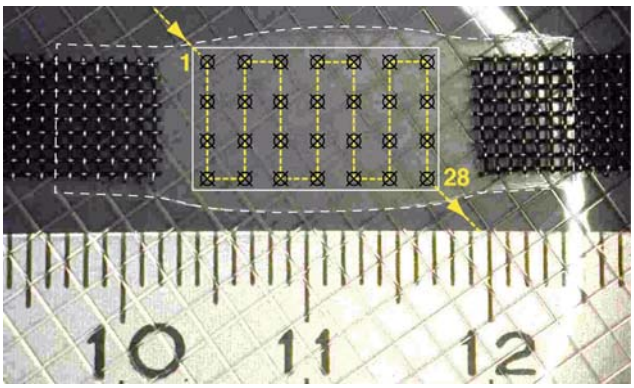

Fig. 6 Representative swollen PEG hydrogel construct. For better visibility, the hydrogel is outlined with a *white dashed line* and the *white box* corresponds to the central region of the FE model (also displayed in Figs. 3–6 in the companion paper (refer to part II)). The 28 symbols indicate the locations where time-lapse sequences were acquired. The yellow path depicts the stage movement pattern from the first to the 28th location

The use of injection molding for preparing the hydrogel samples assured a very high reproducibility of the construct geometry. To enable the transmission of loads to the very soft biomaterial, a stainless-steel mesh was cast-in. The large interfacial area was designed to avoid local stress peaks. For mechanobiological investigations, PEG hydrogels have the important advantage over biopolymers in that the synthetic matrix behaves much like an isotropic Hookean solid whereas biopolymers have a more prominent viscoelastic component (Raeber et al. 2005). At frequencies below 2 Hz (e.g. practicable with the UCSD), the loss modulus G'' of the PEG hydrogels is < 1% of G', indicating that the material behaves nearly ideal elastic. Collagen, for example, exhibits a phase angle $\delta > 20°$ at 1 Hz (Raeber et al. 2005) indicating a considerable time lag between excitation and final material response caused by the viscous component of the material ($\tan\delta$ corresponds to the relative energy loss in the material). Furthermore, the stress-strain relation of cell-populated collagen gels is highly non-linear (Feng et al. 2003). In this case, stress relaxation and creep phenomena have to be expected, which complicate controlled static or dynamic mechanical stimulation. In PEG gels, however, exogenous stretch leads to an immediate, sustained, and reproducible strain state. This was confirmed by 48-h time-lapse sequences of stretched constructs ($\varepsilon = 0.25$) where no drift of embedded beads was seen (not shown). This result indicates that creep phenomena did not take place and that the load transmitting connection between the sample holders and the hydrogel via the mesh was stable.

Besides the possibility of sampling the medium, studies of mechanobiological aspects in cell migration may necessitate

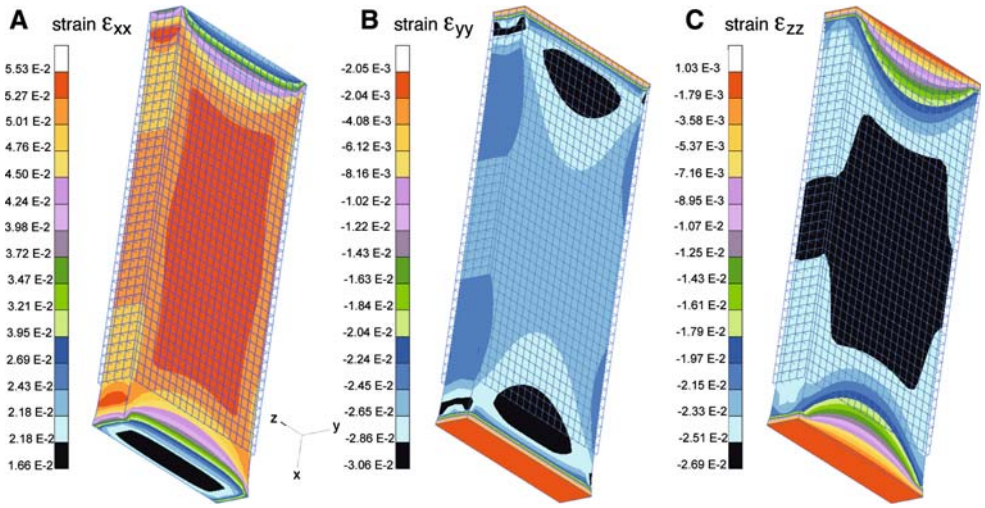

Fig. 7 Static FE analysis showing strains in the x-, y-, and z-direction **(a–c)** of an uniaxially along the x-axis stretched hydrogel construct. The model encompasses the central region shown in Fig. 6 (*white box*) and corresponds to the region of the contour plots in Figs. 3–6 in the companion paper (refer to part II). Note different scales. The meshes used on both sides of the construct for load transmission are complex to model. Therefore, the boundaries of the model are set inside the central part of the construct

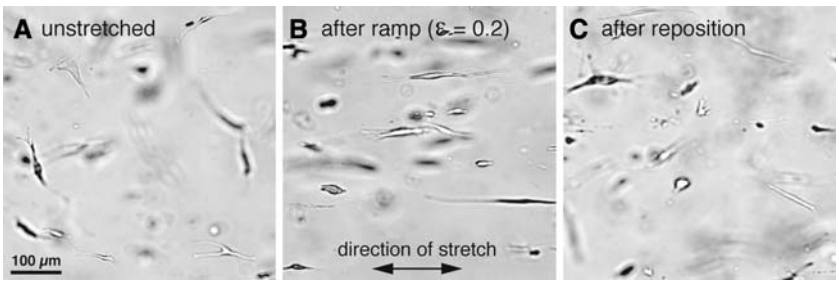

Fig. 8 HFF morphology in the unstretched construct (**a**), 10 h after a maintained single ramp movement inducing 20% strain (**b**), and 8 h after relaxation to the initial strain state (**c**). The images were taken at the center of the construct. Cells align in the direction of the principal strain. This orientation is lost after strain release

biological assays that require the ability to harvest cellular proteins contained on the surface or within the cells. Especially mRNA might be of interest for such studies. Similar to collagen gels, PEG hydrogels can be digested with bacterial collagenases, enabling relatively easy cell harvest. The central region of a single construct (Fig. 6) contains approximately 15,000 cells at normal seeding density (10^5 cells/ml). This moderate cell number will suffice for the detection of mechanically-induced changes in gene expression by rt-PCR but not by Northern blot analysis.

3.4 Finite element (FE) analysis of hydrogel constructs

To further investigate the distribution of stresses and strains within the hydrogel, FE analysis of a PEG construct stretched by a unit displacement was performed (see Fig. 7). The results show that within a central region comprising more than 2/3 of the construct's length, a nearly homogenous strain field can be expected. Contours of constant strain run predominantly in the x-direction, the direction of maximum principal strain. The lateral contraction causes strain and stress components in the y- and the z-direction of approximately half the magnitude of the components along the stretch axis (Fig. 7 b, c, the material was modeled incompressible). Consequently, the residing cells will be subjected to an axial elongation and a lateral compression. Close to the clamping region, the strain field shows considerable gradients pointing towards the center of the displaced boundary. Rheological measurements of PEG hydrogels (Raeber et al. 2005) legitimate the use of linear elasticity theory to model the material.

3.5 Uniaxial stretch induces morphological changes and cellular reorientation parallel to the principal strain axis

As a proof-of-concept, HFF-seeded PEG hydrogel constructs were subjected to a simple stimulation pattern and image sequences were acquired from different locations. The mechanical stimulation consisted of a single step, inducing 20% elongation in the samples followed by an unloading movement 24 h later. Fibroblasts reacted to the applied stretch with a change in morphology and by reorienting along the

main strain axis. Figure 8 shows representative images from the center of a hydrogel construct. In unstretched samples, HFFs had a mixture of stellate and spindle-shaped morphologies, whereas after applying the stretch, cells adopted a more elongated mostly bipolar morphology and aligned parallel to the direction of stretch. This orientation was largely lost when restoring the initial strain state. It has previously been proposed that fibroblasts become oriented parallel with the maximum principal strains in a collagenous 3D environment (Eastwood et al. 1998; Huang et al. 1993; Mudera et al. 2000). The observed thin elongated morphology in combination with the alignment may have reduced the perceived strain across the cell. In effect, fibroblasts appear to be "hiding" from the 3D strain by reducing their cross-sectional area perpendicular to the principal strain. In that way, they only perceive the strain in one direction (Eastwood et al. 1998). Another possible explanation for the noticed behavior could be that cells strengthen contacts and cytoskeleton in the direction of large effective stiffness (Bischofs and Schwarz 2003), which would explain the reorientation parallel to the principal strain. This hypothesis will be further investigated and discussed in detail in the succeeding companion paper (refer to part II). In order to reorient in the MMP-sensitive but otherwise cell-impermeable PEG hydrogels, the cells must perform focalized degradation of the matrix to make room for their elongated cell bodies. This might indicate a controlled interplay between the perception of the mechanical microenvironment and the specific use of the cell's pericellular proteolytic machinery. We observed a rapid reestablishment of a random cellular orientation after unloading the construct (Fig. 8c), similar as observed in collagen gels (Eastwood et al. 1998). This gives further evidence that fibroblasts are mechanosensitive and react repeatedly to changes in their mechanical environment.

Acknowledgments We thank the machine shop crew, particularly F. Brandsberg, ETH Zurich, for invaluable help with the design and for manufacturing most of the UCSD components; Dr. P. Raeber for marvelous artwork; Dr. M. Riner, Precision Implants, Aarau, for help with the FE analysis. Dr. E. Karamuk, Phonak, Stäfa, is acknowledged for constructive early discussions.

References

Akhouayri O, Lafage-Proust M-H, Rattner A, Laroche N, Caillot-Augusseau A, Alexandre C, Vico L (1999) Effects of static or dynamic mechanical stresses on Osteoblast Phenotype expression in three-dimensional contractile collagen gels. J Cell Biochem 76:217–230

Alenghat FJ, Ingber DE (2002) Mechanotransduction: all signals point to cytoskeleton, matrix, and integrins. Sci STKE 2002:PE6

Banes AJ, Link GWJ, Gilbert JW, Tran Son Tay R, Monbureau O (1990) Culturing cells in a mechanically active environment. Am Biotechnol Lab 8:12–22

Barakat A, Lieu D (2003) Differential responsiveness of vascular endothelial cells to different types of fluid mechanical shear stress. Cell Biochem Biophys 38:323–343

Basso N, Heersche JN (2002) Characteristics of in vitro osteoblastic cell loading models. Bone 30:347–351

Bischofs IB, Schwarz US (2003) Cell organization in soft media due to active mechanosensing. Proc Natl Acad Sci U S A 100:9274–9279

Brown TD (2000) Techniques for mechanical stimulation of cells in vitro: a review. J Biomech 33:3–14

Bruinink A, Siragusano D, Ettel G, Brandsberg T, Brandsberg F, Petitmermet M, Muller B, Mayer J, Wintermantel E (2001) The stiffness of bone marrow cell-knit composites is increased during mechanical load. Biomaterials 22:3169–3178

Buckley MJ, Banes AJ, Levin LG, Sumpio BE, Sato M, Jordan R, Gilbert J, Link GW, Tran Son Tay R (1988) Osteoblasts increase their rate of division and align in response to cyclic, mechanical tension in vitro. Bone Miner 4:225–236

Cacou C, Palmer D, Lee DA, Bader DL, Shelton JC (2000) A system for monitoring the response of uniaxial strain on cell seeded collagen gels. Med Eng Phys 22:327–333

Carvalho RS, Scott JE, Suga DM, Yen EH (1994) Stimulation of signal transduction pathways in osteoblasts by mechanical strain potentiated by parathyroid hormone. J Bone Miner Res 9:999–1011

Duncan R, Turner C (1995) Mechanotransduction and the functional response of bone to mechanical strain. Calcif Tissue Int 57: 344–358

Duncan RL, Hruska KA (1994) Chronic, intermittent loading alters mechanosensitive channel characteristics in osteoblast-like cells. Am J Physiol 267:F909–F916

Eastwood M, McGrouther DA, Brown RA (1994) A culture force monitor for measurement of contraction forces generated in human dermal fibroblast cultures: evidence for cell-matrix mechanical signalling. Biochim Biophys Acta 1201:186–192

Eastwood M, Mudera VC, McGrouther DA, Brown RA (1998) Effect of precise mechanical loading on fibroblast populated collagen lattices: morphological changes. Cell Motil Cytoskeleton 40:13–21

Feng Z, Yamato M, Akutsu T, Nakamura T, Okano T, Umezu M (2003) Investigation on the mechanical properties of contracted collagen gels as a scaffold for tissue engineering. Artif Organs 27:84–91

Fung Y-C (1990) Biomechanics motion, flow, stress, and growth. Springer, New York

Fung Y-C (1993) Biomechanics mechanical properties of living tissues. Springer, New York

Hern DL, Hubbell JA (1998) Incorporation of adhesion peptides into nonadhesive hydrogels useful for tissue resurfacing. J Biomed Mater Res 39:266–276

Huang D, Chang TR, Aggarwal A, Lee RC, Ehrlich HP (1993) Mechanisms and dynamics of mechanical strengthening in ligament-equivalent fibroblast-populated collagen matrices. Ann Biomed Eng 21:289–305

Ingber DE (1997) Tensegrity: the architectural basis of cellular mechanotransduction. Annu Rev Physiol 59:575–599

Jones DB, Nolte H, Scholübbers J-G, Turner E, Veltel D (1991) Biochemical signal transduction of mechanical strain in osteoblast-like cells. Biomaterials 12:101–110

Katsumi A, Orr AW, Tzima E, Schwartz MA (2004) Integrins in mechanotransduction. J Biol Chem 279:12001–12004

Kim BS, Mooney DJ (2000) Scaffolds for engineering smooth muscle under cyclic mechanical strain conditions. J Biomech Eng 122:210–215

Knezevic V, Sim AJ, Borg TK, Holmes JW (2002) Isotonic biaxial loading of fibroblast-populated collagen gels: a versatile, low-cost system for the study of mechanobiology. Biomech Model Mechanobiol 1:59–67

Ku DN, Zhu C (1993) The Mechanical Environment of the Artery. In: Sumpio BE (ed) Hemodynamic forces and vascular cell biology. R.G. Landes Company, Austin, pp 1–23

Langelier E, Rancourt D, Bouchard S, Lord C, Stevens PP, Germain L, Auger FA (1999) Cyclic traction machine for long-term culture of fibroblast-populated collagen gels. Ann Biomed Eng 27:67–72

Lee AA, Graham DA, Dela Cruz S, Ratcliffe A, Karlon WJ (2002) Fluid shear stress-induced alignment of cultured vascular smooth muscle cells. J Biomech Eng 124:37–43

Lutolf MP, Hubbell JA (2003) Synthesis and physicochemical characterization of end-linked poly(ethylene glycol)-co-peptide hydrogels formed by Michael-type addition. Biomacromolecules 4:713–722

Lutolf MP, Lauer-Fields JL, Schmoekel HG, Metters AT, Weber FE, Fields GB, Hubbell JA (2003a) Synthetic matrix metalloproteinase-sensitive hydrogels for the conduction of tissue regeneration: engineering cell-invasion characteristics. Proc Natl Acad Sci USA 100:5413–5418

Lutolf MP, Raeber GP, Zisch AH, Tirelli N, Hubbell JA (2003b) Cell-responsive synthetic hydrogels. Adv Mater 15:888–892

Matsuda N, Morita N, Matsuda K, Watanabe M (1998) Proliferation and differentiation of human osteoblastic cells associated with differential activation of MAP kinases in response to epidermal growth factor, hypoxia, and mechanical stress in vitro. Biochem Biophys Res Commun. 249:350–354

Mitchell SB, Sanders JE, Garbini JL, Schuessler PK (2001) A device to apply user-specified strains to biomaterials in culture. IEEE Trans Biomed Eng 48:268–273

Mudera VC, Pleass R, Eastwood M, Tarnuzzer R, Schultz G, Khaw P, McGrouther DA, Brown RA (2000) Molecular responses of human dermal fibroblasts to dual cues: contact guidance and mechanical load. Cell Motil Cytoskeleton 45:1–9

Nishioka S, Fukuda K, Tanaka S (1993) Cyclic stretch increases alkaline phosphatase activity of osteoblast-like cells: a role for prostaglandin E2. Bone Miner 21:141–150

Patel DJ, Greenfield JC, Jr., Austen WG, Morrow AG, Fry DL (1965) Pressure-flow relationships in the ascending aorta and femoral artery of man. J Appl Physiol 20:459–463

Pierschbacher MD, Ruoslahti E (1984) Cell attachment activity of fibronectin can be duplicated by small synthetic fragments of the molecule. Nature 309:30–33

Prajapati RT, Chavally-Mis B, Herbage D, Eastwood M, Brown RA (2000) Mechanical loading regulates protease production by fibroblasts in three-dimensional collagen substrates. Wound Repair Regen 8:226–237

Putnam AJ, Schultz K, Mooney DJ (2001) Control of microtubule assembly by extracellular matrix and externally applied strain. Am J Physiol Cell Physiol 280:C556–C564

Raeber GP, Lutolf MP, Hubbell JA (2005) Molecularly engineered PEG hydrogels: a novel model system for proteolytically-mediated cell migration. Biophys J 89:1374–1388

Sachs F, Morris CE (1998) Mechanosensitive ion channels in nonspecialized cells. Rev Physiol Biochem Pharmacol 132:1–77

Sheetz MP, Felsenfeld DP, Galbraith CG (1998) Cell migration: regulation of force on extracellular-matrix-integrin complexes. Trends Cell Biol 8:51–54

Tang LL, Wang YL, Sun CX (2004) The stress reaction and its molecular events: splicing variants. Biochem Biophys Res Commun 320:287–291

Turner CH, Owan I, Takano Y (1995) Mechanotransduction in bone: role of strain rate. Am J Physiol 269:E438–E442